

Hugues Cabane · Didier Laporte · Ariel Provost

An experimental study of Ostwald ripening of olivine and plagioclase in silicate melts: implications for the growth and size of crystals in magmas

Received: 10 August 2004 / Accepted: 03 May 2005 / Published online: 2 July 2005
© Springer-Verlag 2005

Abstract We carried out an experimental study to characterize the kinetics of Ostwald ripening in the forsterite-basalt system and in the plagioclase (An_{65})-andesite system. Eight experiments were done in each system to monitor the evolution of mean grain size and crystal size distribution (CSD) with time t ; the experiments were performed in a 1-atmosphere quench furnace, at 1,250°C for plagioclase and 1,300°C for olivine. Very contrasted coarsening kinetics were observed in the two series. In the plagioclase series, the mean grain size increased as $\log(t)$, from $\approx 3 \mu\text{m}$ to only $8.7 \mu\text{m}$ in 336 h. The kinetic law in $\log(t)$ means that Ostwald ripening was rate-limited by surface nucleation at plagioclase-liquid interfaces. In the olivine series, the mean grain size increased as $t^{1/3}$, from $\approx 3 \mu\text{m}$ to $23.2 \mu\text{m}$ in 496 h. A kinetic law in $t^{1/3}$ is expected when Ostwald ripening is rate-limited either by diffusion in the liquid or by grain growth/dissolution controlled by a screw dislocation mechanism. The shape of olivine CSDs, in particular their positive skewness, indicates that grain coarsening in the olivine experiments was controlled by a screw dislocation mechanism, not by diffusion. As the degrees of undercooling ΔT (or supersaturation) involved in Ostwald ripening are essentially $< 1^\circ\text{C}$, the mechanisms of crystal growth identified in our experiments are expected to be those prevailing during the slow crystallisation of large magma chambers. We extrapolated our experimental data to geological time scales to

estimate the effect of Ostwald ripening on the size of crystals in magmas. In the case of plagioclase, Ostwald ripening is only efficient for mean grain sizes of a few microns to $20 \mu\text{m}$, even for a time scale of 10^5 years. It can, however, result in a significant decrease of the number of small crystals per unit volume, and contribute to the development of convex upwards CSDs. For olivine, the mean grain size increases from $2\text{--}3 \mu\text{m}$ to $\approx 70 \mu\text{m}$ in 1 year and $700 \mu\text{m}$ in 10^3 years; a mean grain size of 3mm is reached in 10^5 years. Accordingly, the rate of grain size-dependent processes, such as compaction of olivine-rich cumulates or melt extraction from partially molten peridotites, may significantly be enhanced by textural coarsening.

Introduction

In a system consisting of solid grains in a liquid at chemical equilibrium, large grains grow with time at the expense of the small ones, a process known as Ostwald ripening (Ostwald 1901). The driving force is the reduction of the excess energy associated with solid-liquid interfaces. Ostwald ripening results in an increase of the mean grain size and a decrease of the number of grains per unit volume, but the total volume of each phase remains essentially constant during the process. Through its effect on grain size, Ostwald ripening could increase significantly the rate of many magmatic processes, including the segregation of a magma from its source or crystal settling in a magma chamber. Indeed, one of the main physical properties controlling the rate of magma segregation is permeability, which is proportional to the square of the grain size of the partially molten rock. Similarly, the terminal velocity of a falling crystal is proportional to the square of its size. The actual influence of Ostwald ripening on the dynamics of magmatic processes will be a function of its kinetics, which constitutes the main objective of our study.

Communicated by Timothy L. Grove

H. Cabane · D. Laporte (✉) · A. Provost
Laboratoire Magmas et Volcans, CNRS/Université Blaise Pascal/
IRD, OPGC, 5 rue Kessler, 63038, Clermont-Ferrand Cedex,
France
E-mail: laporte@opgc.univ-bpclermont.fr
Tel.: +33-4-73346733
Fax: +33-4-73346744

Present address: H. Cabane
Saint-Gobain Cristaux et Détecteurs, BP
521, 77794, Nemours cédex, France

The second objective of this study was more exploratory: as the only driving force for grain coarsening is the reduction of interfacial energies, the degrees of supersaturation involved in Ostwald ripening are very small, and equivalent to undercoolings $\leq 1^\circ\text{C}$. Accordingly, the kinetics of Ostwald ripening may provide first order constraints on the mechanisms and rates of crystal growth at the very low degrees of undercooling prevailing in large magma bodies. By comparison, crystal growth data cannot be directly obtained experimentally at undercoolings $\leq 10^\circ\text{C}$ (e.g., Kirkpatrick 1981).

The kinetics of Ostwald ripening can be controlled either by the diffusion rate of matter between large and small grains or by the rates of growth or dissolution at solid-liquid interfaces (Wagner 1961). Depending on which mechanism controls the kinetics, the mean grain size may increase as $t^{1/2}$, $t^{1/3}$, $\log(t)$, where t stands for time (see below). As in Earth Sciences, results need to be extrapolated from relatively short experiments (hours to weeks) to time scales of years to millions of years, it is critical to determine precisely the kind of rate law followed by the mean grain size. We carried out an experimental study to characterise the kinetics of Ostwald ripening in three major silicate systems: the quartz-granite system, the olivine-basalt system, and the plagioclase-andesite system. The results obtained in the quartz-granite system were presented in a previous paper (Cabane et al. 2001). In this paper, the experimental results obtained in the olivine-basalt and plagioclase-andesite systems are summarised and their implications for magmatic processes are discussed.

Ostwald ripening: theoretical background

Driving forces

The fundamental relationship behind Ostwald ripening is the Gibbs-Thomson equation, which relates chemical potential to interfacial curvature (e.g., Bulau et al. 1979). Let us consider a two-phase system composed of grains of phase β dispersed in a liquid phase α , at a constant temperature T . We assume that the grains are spherical, and that the solid-liquid interfacial energy per unit area, $\sigma_{\alpha\beta}$ (J/m^2), is isotropic, that is, the value of $\sigma_{\alpha\beta}$ does not depend on the orientation of the interface relative to the grain lattice. In addition, the system contains only two chemical components, A and B, and phase β is made purely of B. The relationship between pressures in phases α and β is given by Laplace's law $P_\beta - P_\alpha = 2\sigma_{\alpha\beta}/r$, where r is the radius of the grain under consideration. The Gibbs-Thomson equation shows that the chemical potential of component B in phase β , $\mu_{\beta\text{B}}$ (T, P_β), is a function of radius r :

$$\mu_{\beta\text{B}}(T, P_\beta) = \mu_{\beta\text{B}}(T, P_\alpha) + \frac{2\sigma_{\alpha\beta}V_\beta}{r}, \quad (1)$$

where V_β is the molar volume of β . Assuming that the liquid is an ideal solution, the chemical potential of B in α is:

$$\mu_{\alpha\text{B}}(T, P_\alpha, C) = \mu_{\alpha\text{B}}^0(T, P_\alpha) + R_g T \ln(C), \quad (2)$$

where $\mu_{\alpha\text{B}}^0$ is the chemical potential of a liquid of pure composition B, R_g is the gas constant, and C is the local mole fraction of B in the liquid. The liquid is in equilibrium with a grain of radius r for a unique value of C , referred to as $C_{\text{sat}}(r)$, such that $\mu_{\beta\text{B}}(T, P_\beta) = \mu_{\alpha\text{B}}(T, P_\alpha, C_{\text{sat}}(r))$. Substituting Eqs. 1 and 2, we obtain:

$$R_g T \ln(C_{\text{sat}}(r)) - \frac{2\sigma_{\alpha\beta}V_\beta}{r} = \mu_{\beta\text{B}}(T, P_\alpha) - \mu_{\alpha\text{B}}^0(T, P_\alpha). \quad (3)$$

Introducing $C_0 = C_{\text{sat}}(r \rightarrow \infty)$, the concentration of B in the liquid in equilibrium with a grain of infinite radius, Eq. 3 reads:

$$\ln \frac{C_{\text{sat}}(r)}{C_0} = \frac{r_0}{r}, \quad (4)$$

where $r_0 = 2\sigma_{\alpha\beta}V_\beta/R_g T$ is a constant with the dimension of a length.

The LSW theory is based on a mean field approximation of Ostwald ripening (Lifshitz and Slyozov 1961; Wagner 1961): (1) far from any grain, the liquid is supposed to have a uniform concentration, C_1 ; (2) each grain interacts only with this liquid, not with the neighboring grains. At this point, it is convenient to introduce the critical radius, r^* , which is defined as the radius of a grain in equilibrium with a liquid of concentration C_1 :

$$r^* = \frac{r_0}{\ln(C_1/C_0)}. \quad (5)$$

The difference $\Delta C(r) = C_{\text{sat}}(r) - C_1 = C_{\text{sat}}(r) - C_{\text{sat}}(r^*)$ is the driving force of Ostwald ripening. Grains of radius $r = r^*$ neither grow nor dissolve ($\Delta C(r^*) = 0$). Equations 4 and 5 show that $\Delta C(r) < 0$ for $r > r^*$, and $\Delta C(r) > 0$ for $r < r^*$. Accordingly, the large grains ($r > r^*$) will grow while the small ones ($r < r^*$) will dissolve into the liquid. Note that concentration C_1 is not constant: it decreases very slightly with time due to grain coarsening, and the critical radius r^* increases concurrently.

The driving force for coarsening may be recast in terms of the undercooling experienced by a crystal of radius r : $\Delta T(r) = T_f(r) - T$ where $T_f(r)$ stands for the temperature at which the crystal would be in equilibrium with the liquid (of concentration C_1), and T is the actual temperature. The equation for $T_f(r)$ is obtained by equating Eq. 1 with Eq. 2:

$$\mu_{\beta\text{B}}(T_f(r), P_\alpha) + \frac{2\sigma_{\alpha\beta}V_\beta}{r} = \mu_{\alpha\text{B}}^0(T_f(r), P_\alpha) + R_g T_f(r) \ln(C_1). \quad (6)$$

This equation also gives $T_f(r^*) = T$ and $T_f(r \rightarrow \infty) = T_L$, the liquidus temperature. Combining these three variants of Eq. 6 gives:

$$\Delta T(r) = \frac{2\sigma_{\alpha\beta}V_{\beta}T_L}{\Delta H_f} \left(\frac{1}{r^*} - \frac{1}{r} \right) = \frac{R_g T T_L}{\Delta H_f} \left(\frac{r_0}{r^*} - \frac{r_0}{r} \right), \quad (7)$$

where ΔH_f , the latent heat of fusion of pure B, comes from the thermodynamic equation $\mu_{\alpha,B}^0(T_L, P_{\alpha}) - \mu_{\beta,B}(T_L, P_{\alpha}) = \Delta H_f - T_L \Delta S_f$ (ΔS_f being the entropy of fusion).

As an illustration, we computed $\Delta T(r)$ in a system with a critical radius r^* equal to 5 μm , a typical value in our experiments. For the main physical parameters, we used values corresponding to our plagioclase series: $T_L \approx T = 1,523 \text{ K}$; $V_{\beta} = 0.000101 \text{ m}^3/\text{mol}$; $\sigma_{\alpha\beta} = 0.5 \text{ J/m}^2$; $\Delta H_f = 70,000 \text{ J/mol}$ (with these values, length r_0 in Eq. 4 is equal to 8 nm). The undercooling $\Delta T(r)$ is plotted as a function of grain size $2r$ (i.e., diameter) in Fig. 1. Because the only driving force is the reduction of interfacial energies, the absolute values of ΔT involved in Ostwald ripening are small: (1) grains larger than the critical size, $2r^*$, grow but at an undercooling $< 1^{\circ}\text{C}$; and (2) the liquid is superheated with respect to grains smaller than $2r^*$ (that is, $\Delta T < 0$), but by only a few degrees for a grain size of 1 μm and by a few tens of degrees for a grain size of 0.1 μm .

Mechanisms controlling the rate of Ostwald ripening

The kinetics of Ostwald ripening may be controlled either by the attachment/detachment of atoms at the crystal-melt-interface or by diffusion of components in

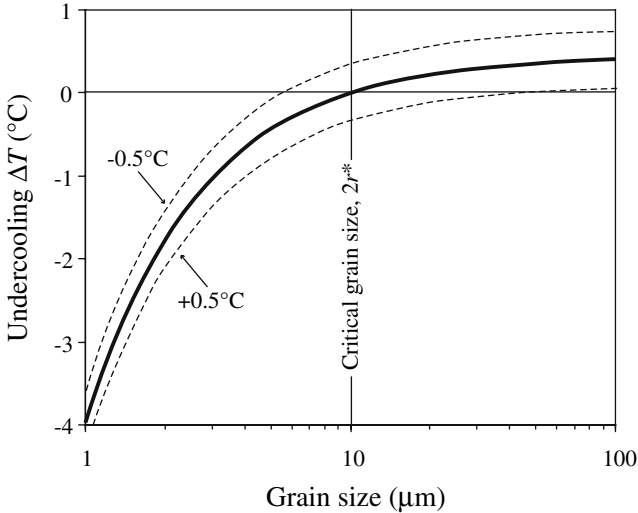


Fig. 1 Undercooling ΔT as a function of grain diameter in a system undergoing Ostwald ripening (solid line): the liquid is supersaturated ($\Delta T > 0^{\circ}\text{C}$) with respect to grains larger than the critical size, $2r^*$ (here taken as 10 μm , a typical value in our experiments), but undersaturated ($\Delta T < 0^{\circ}\text{C}$) with respect to grains smaller than $2r^*$. A sudden change of temperature of $+0.5^{\circ}\text{C}$ or -0.5°C will slightly shift the ΔT versus $2r$ curves downwards or upwards, respectively (dashed lines; see the discussion section)

the melt to and from the interface. When the rates of crystal growth or dissolution are fast relative to diffusion, concentration gradients build up in the melt around the crystals and the rate of grain coarsening is controlled by the rate of diffusion in the melt. When diffusive transfer is sufficiently rapid to prevent concentration gradients to build up in the melt close to the crystal-melt interface, the coarsening rate is controlled by the mechanisms of crystal growth or dissolution. Three kinds of interface controlled ripening may be distinguished depending on the structure of the solid-melt interface and the nature of the growth mechanism: continuous growth, surface nucleation, and spiral growth (for reviews on crystal growth mechanisms, see Kirkpatrick 1975, 1981; Baronnet 1984; Lasaga 1998). The main features of the four kinds of Ostwald ripening are summarized below:

1. *Diffusion control.* When Ostwald ripening is controlled by diffusion through the liquid, the mean grain size obeys a law of the form:

$$\bar{d}^n - \bar{d}_0^n = k \cdot t \quad (8)$$

where \bar{d} is the mean grain size at time t , \bar{d}_0 is the initial mean grain size (at $t=0$), k is the ripening rate (in $\text{length}^n \times \text{time}^{-1}$), and the exponent n is equal to 3 (Lifshitz and Slyozov 1961; Wagner 1961; Dehoff 1991). The ripening rate is a function of the effective diffusion coefficient D , solid-liquid interfacial energy, temperature, etc., and the exact expression for the kinetic law is:

$$\bar{d}^3 - \bar{d}_0^3 = \frac{64D\sigma_{\alpha\beta}V_{\beta}c_0}{9R_gT} t, \quad (9)$$

where c_0 is the mass fraction of component B in the liquid in equilibrium with a grain of infinite radius.

2. *Continuous growth control.* Equation 8 also applies to the case where Ostwald ripening is controlled by continuous growth/dissolution, but the exponent n is now equal to 2 (Wagner 1961; Dehoff 1984).
3. *Surface nucleation control.* Surface nucleation is one type of layer growth (or lateral growth). In layer growth, the solid-melt interface is assumed to be atomically flat except at steps, at which the atoms can attach to the growing surface. In the case of surface nucleation, one atom thick clusters nucleate on the former surface and then spread laterally over the surface as atoms attach to their edges. For surface nucleation controlled Ostwald ripening, Solomatov and Stevenson (1993) obtained a logarithmic dependence of the mean grain size with time:

$$\bar{d} - \bar{d}_0 = k_1 \log \left(1 + \frac{t}{\tau} \right), \quad (10)$$

where k_1 and τ are constants, with the dimensions of a length and a time, respectively.

4. *Spiral growth control.* Spiral growth is the second type of layer growth. It is related to the emergence on the growing surface of a screw dislocation, which

creates a self-perpetuating step in the shape of a spiral. When Ostwald ripening is controlled by the operation of screw dislocations, the mean grain size obeys Eq. 8, with an exponent n equal to 3 (as in the case of a diffusion control; Chai 1974; Kahlweit 1975; Ratke et al. 1995).

In the case of a crystal growing from the melt (Kirkpatrick 1975, 1981; Dowty 1980; Lasaga 1998), interfacial processes are expected to be rate controlling at small undercoolings because the growth rate is small and the diffusion coefficient is large. With increasing undercooling, the growth rate increases and the diffusion coefficient decreases (due to decreasing temperature), and at some point, crystal growth may become diffusion controlled. For instance, the growth of plagioclase crystals (An₁₀₋₄₀) in the albite-anorthite system at 1 atm is controlled by crystal-melt interfacial processes for $\Delta T < 20^\circ\text{C}$ (Muncill and Lasaga 1987). By analogy, Ostwald ripening in silicate systems will presumably be rate-limited by interfacial processes, not by diffusion, because the degrees of undercooling/superheating involved are extremely small (Fig. 1), leading to commensurately small rates of grain growth/dissolution. In addition, we anticipate that the mechanisms controlling Ostwald ripening in silicate systems should be layer growth, rather than continuous growth. Indeed, it has been observed experimentally that crystals exhibiting faceted morphologies, like most silicates, are produced by a layer growth mechanism, while rounded, non-faceted crystals are the result of continuous growth (Jackson et al. 1967).

Experimental and analytical techniques

Starting materials

Forsterite-Basalt system

A first series of experiments was performed in the system forsterite-basalt at 1 atm–1,300°C, with durations ranging from <1 h to 496 h (runs Ol#5 to Ol#12, Table 1). The starting material was a mixture of 53 wt% forsterite and 47 wt% basalt glass CMAS2 (Table 2). The reason why we used a relatively large proportion of olivine was to prevent crystal settling during the long duration experiments, a problem encountered in a previous study of Ostwald ripening in the olivine-basalt system (with 10 vol.% olivine; Park and Hanson 1999). Our forsterite powder was produced from a Mg₂SiO₄ gel by hydrothermal synthesis in a piston-cylinder apparatus at 1 GPa–1,000°C (15 wt% water was added to the gel to promote crystallisation; run duration was 117 h). The resulting powder was very fine, with grains of a few microns. In addition to forsterite, it contained a small amount of enstatite (detected by X-ray diffraction). This powder was slightly ground in ethanol and then fired at 1 atm–1,000°C for 17 h.

Table 1 A summary of run information and main textural parameters

	Duration (h)	N^a	v_{xt}^b (vol.%)	\bar{d}_{2D}^c (μm)	\bar{d}_{3D}^d (μm)	N_v (mm^{-3})
Ol#12 ^e	0.33	–	–	–	≈3	–
Ol#8	1.33	339	44	4.2 (0.53)	3.7	4.82×10 ⁶
Ol#11	6.08	352	48	5.7 (0.59)	5.8	3.18×10 ⁶
Ol#9	15.40	417	53	8.4 (1.04)	7.5	1.19×10 ⁶
Ol#5	43.20	366	53	13.2 (1.33)	13.3	3.63×10 ⁵
Ol#6	90.43	325	50	14.8 (1.65)	14.2	2.21×10 ⁵
Ol#7	161.80	313	47	18.8 (2.01)	19.3	8.25×10 ⁴
Ol#10	496.38	313	53	25.5 (2.70)	23.2	4.23×10 ⁴
Pl#8	1.00	193	17	2.2 (0.35)	3.4	5.65×10 ⁶
Pl#7	3.30	210	17	2.9 (0.35)	6.0	2.72×10 ⁶
Pl#5	9.60	138	15	3.4 (0.46)	5.2	1.95×10 ⁶
Pl#2	20.00	228	19	3.7 (0.48)	6.3	9.51×10 ⁵
Pl#6	45.42	319	20	3.8 (0.49)	6.7	7.99×10 ⁵
Pl#9	75.00	265	12	4.3 (0.53)	7.8	1.18×10 ⁶
Pl#4	150.00	180	21	4.4 (0.53)	7.6	9.66×10 ⁵
Pl#3	336.00	428	17	5.2 (0.72)	8.7	2.30×10 ⁵

All the experiments were made in a 1 atm quench furnace. Run temperature was 1,300°C in the olivine experiments (Ol#5 to Ol#12), and 1,250°C in the plagioclase experiments (Pl#2 to Pl#9). The solid phase was pure forsterite in the olivine experiments, and labradorite (An₆₃₋₆₄) in the plagioclase experiments

^a N is the number of grain sections measured

^bThe volume fraction of crystals, v_{xt} , is considered to be equal to the surface fraction of crystals in polished sections; the error on v_{xt} is approximately ± 3 vol.%

^c \bar{d}_{2D} is the 2D mean grain size. The error on the mean is given in parentheses: it is equal to $2s/N^{1/2}$ (where s is the standard deviation of the 2D grain size distribution) plus twice the size of a pixel in the back-scattered electron images used for textural analysis (see text for details). Pixel size was: 0.10 μm in Pl#5, 7, 8; 0.13 μm in Ol#8 and Pl#2, 4; 0.16 μm in Ol#11 and Pl#6; 0.18 μm in Pl#9; 0.26 μm in Ol#9 and Pl#3; 0.35 μm in Ol#5; 0.39 μm in Ol#6; 0.52 μm in Ol#7; 0.63 μm in Ol#10

^dStereological corrections were applied to 2D CSDs to estimate the 3D mean grain sizes, \bar{d}_{3D} , and the numbers of grains per unit volume, N_v . In the olivine experiments, we assumed a spherical grain shape and we applied Saltykov corrections (Saltykov 1967). In the plagioclase experiments, grain shape was assumed to be a rectangular parallelepiped, and we used the program ‘‘CSD Corrections’’ (Higgins 2000)

^eThe texture in sample Ol#12 was not quantified because of the very small grain size

Basalt CMAS2 used in the olivine-basalt experiments has a composition of 42 wt % An – 50 wt % Di – 8 wt % Fo (An, Di, Fo stand for anorthite, diopside, and forsterite, respectively; for the composition in oxides, see Table 2). It was obtained by melting a mixture of An, Di and Fo gels at 1 atm–1,450°C for 1 h. The resulting glass was ground in a micronising mill to reduce the fragments to ≤ 20 μm . The 1-atm liquidus temperature of composition CMAS2 is $\approx 1,280^\circ\text{C}$ and the liquidus phase is Fo (for liquidus phase relations on the join Di-Fo-An, see Presnall et al. 1978). As the composition CMAS2 is very close to the Di-Fo-An cotectic at 1 atm, we decided to perform the olivine-basalt experiments at 1,300°C instead of 1,280°C, to prevent crystallisation of Di or An. In addition, this excess in temperature will allow the dissolution of the traces of enstatite present in the olivine powder. A small amount of Fo is also ex-

Table 2 Mean glass compositions (wt%) in the olivine experiments

	MgO	Al ₂ O ₃	CaO	SiO ₂	A. T.
CMAS2 ^a	12.5	15.4	21.4	50.7	–
Ol#12 (7)	14.68 (16)	14.76 (12)	19.63 (16)	50.92 (15)	99.83
Ol#8 (7)	14.61 (13)	15.11 (33)	19.71 (21)	50.57 (25)	99.41
Ol#11 (6)	14.71 (6)	14.87 (19)	19.64 (16)	50.78 (18)	99.59
Ol#9 (7)	14.61 (11)	14.66 (16)	19.65 (14)	51.08 (19)	99.57
Ol#5 (7)	14.41 (15)	14.84 (14)	19.74 (12)	51.02 (10)	99.61
Ol#6 (8)	14.47 (8)	14.78 (13)	19.68 (11)	51.06 (16)	99.55
Ol#7 (7)	14.53 (13)	14.60 (7)	19.59 (15)	51.28 (11)	99.39
Ol#10 (7)	14.64 (18)	14.73 (11)	19.67 (10)	50.96 (18)	99.39

Glass compositions were determined by electron probe micro-analysis (conditions: 15 kV, 8 nA, counting times of 10 s, and beam size equal to 5×5 μm). The number of analyses per sample is given in parentheses after the run number. The numbers in parentheses after the mean values are 1σ standard deviations, given in terms of the least unit cited: e.g., 14.41 (15) represents 14.41 ± 0.15. All compositions are normalized to a sum of 100 wt% (analytical totals are shown for information in column “A. T.”)

^aComposition computed from the mass fractions of An, Di, and Fo gels (0.42, 0.50, and 0.08, respectively) in synthetic basalt CMAS2

pected to be dissolved into the liquid in the early stages of the experiments at 1,300°C.

Plagioclase-Andesite system

A second series of experiments was performed in the system plagioclase-andesite at 1 atm–1,250°C, with durations ranging from 1 h to 336 h (runs Pl#2 to Pl#9, Table 1). The starting material was a mixture of 20 wt%

labradorite and 80 wt% andesite glass CMASN (Table 3). The plagioclase powder was produced by grinding fragments of a labradorite crystal from an anorthosite of the Grenville province, Quebec, whose composition was An₆₄. The mineral was dark because of the presence of minute inclusions of quartz, amphibole, and magnetite. As the mass fraction of inclusions was very small, the departure from nominal composition An₆₄ was marginal except for a slight contamination in iron (detected in the experimental glasses; Table 3). The plagioclase was ground to reduce the grain size to less than 10 μm, but most grains were ≤ 1 μm.

The composition of andesite glass CMASN is 25.4 wt% An – 45.1 wt% albite (Ab) – 29.5 wt% Di. In terms of oxide concentrations (Table 3), it is close to average andesite except that it is iron-free and that it contains about twice as much CaO as typical andesites. Glass CMASN was obtained by melting a mixture of Ab, An, and Di gels at 1 atm–1,430°C for 1 h. The resulting glass was reduced to fragments ≤ 10 μm in a micronising mill. It was then mixed with the plagioclase powder, and the mixture was fired at 850°C for 2 h. Composition CMASN was chosen because it is in equilibrium at 1 atm–1,250°C with a plagioclase of composition An_{64.5} (Weill et al. 1980), that is, almost exactly the composition of our natural plagioclase. Another advantage of this composition is its relatively large viscosity: ≈250 Pa.s at 1,250°C, which results in a negligible settling velocity of the plagioclase crystals (for a grain size < 10 μm). Accordingly, plagioclase and liquid

Table 3 Average compositions of glasses and crystals (wt%) in the plagioclase experiments

	SiO ₂	MgO	FeO	Na ₂ O	CaO	Al ₂ O ₃	A. T.
Glass							
CMASN ^a	58.3	5.5	–	5.3	12.8	18.1	–
Pl#8 (7)	59.34 (40)	5.33 (28)	0.35 (6)	5.29 (23)	11.81 (16)	17.89 (54)	100.19
Pl#7 (7)	59.47 (26)	5.38 (12)	0.35 (3)	5.23 (12)	11.83 (21)	17.74 (10)	100.28
Pl#5 (6)	59.17 (11)	5.54 (7)	0.38 (4)	5.41 (8)	11.80 (15)	17.69 (18)	100.02
Pl#2 (6)	59.62 (35)	5.39 (9)	0.34 (3)	5.31 (14)	11.67 (14)	17.66 (8)	100.65
Pl#6 (6)	59.71 (21)	5.42 (12)	0.36 (8)	5.26 (1)	11.61 (8)	17.63 (16)	100.10
Pl#9 (4)	59.26 (18)	5.56 (4)	0.33 (9)	5.39 (10)	11.70 (20)	17.76 (21)	99.01
Pl#4 (5)	59.68 (15)	5.34 (8)	0.25 (3)	5.43 (9)	11.57 (20)	17.74 (15)	99.93
Pl#3 (7)	59.25 (17)	5.59 (5)	0.34 (6)	5.39 (16)	11.70 (13)	17.73 (12)	99.25
Plagioclase							
Labrad. ^b	51.63 (38)	0.01 (1)	0.26 (32)	4.17 (10)	12.82 (16)	29.45 (34)	98.56
Pl#8 (2)	53.78 (8)	0.83 (10)	0.09 (9)	4.16 (10)	12.91 (22)	28.24 (59)	99.69
Pl#7 (3)	53.07 (38)	0.18 (12)	0.12 (7)	4.15 (17)	12.95 (44)	29.53 (4)	100.60
Pl#5 (5)	52.93 (49)	0.37 (27)	0.11 (4)	4.20 (7)	13.00 (25)	29.38 (64)	100.11
Pl#2 (5)	52.92 (26)	0.21 (14)	0.08 (5)	4.23 (7)	13.05 (23)	29.51 (37)	100.36
Pl#6 (3)	52.95 (23)	0.16 (9)	0.08 (1)	4.16 (12)	13.09 (22)	29.56 (11)	99.68
Pl#9 (3)	52.96 (9)	0.20 (4)	0.04 (4)	4.09 (2)	13.05 (11)	29.66 (8)	99.46
Pl#4 (5)	52.80 (32)	0.22 (13)	0.04 (2)	4.02 (26)	13.33 (40)	29.59 (35)	99.89
Pl#3 (5)	52.58 (29)	0.25 (10)	0.10 (2)	4.13 (11)	13.08 (28)	29.86 (24)	99.92

Phase compositions were determined by electron probe micro-analysis. The analytical conditions for crystals were 15 kV, 15 nA, counting times of 10 s, and a focussed beam. For glasses, the analytical conditions were 15 kV, 8 nA, counting times of 10 s, and a beam size equal to 10×10 μm (Pl#3, Pl#5, Pl#9) or 5×5 μm (Pl#2, Pl#4, Pl#6, Pl#7, Pl#8). The number of analyses per sample is given in parentheses after the run number. The numbers in parentheses after the mean values are 1σ standard deviations, given in terms of

the least unit cited. All compositions are normalized to a sum of 100 wt% (analytical totals are shown for information in column “A. T.”)

^aComposition computed from the mass fractions of An, Ab, and Di gels (0.254, 0.451, and 0.295, respectively) in synthetic andesite CMASN

^bMean values of 10 analyses of the natural labradorite crystal (Grenville province, Quebec) used as starting material

cannot separate under the effect of gravity, despite the relatively low volume fraction of crystals in the plagioclase-andesite experiments.

Experimental techniques

All the experiments were made in a 1-atm quench furnace. Twenty milligram aliquots of the starting powders were loaded into platinum capsules (outer diameter, 3 mm; wall thickness, 0.2 mm). For the olivine experiments, the capsules were left open because there was no volatile elements in the system. For the plagioclase experiments, the capsules were arc-welded to avoid sodium loss. At the beginning of an experiment, the capsule was suspended with a platinum wire to an alumina sample holder (also hosting the thermocouple); the sample holder was then brought down into the furnace until the sample reached the hot spot. The target temperature was reached in 15 min for the plagioclase experiments and 3 min for the olivine experiments (the two series were run in two different furnaces). Temperature was controlled by a Pt₉₄Rh₆/Pt₇₀Rh₃₀ thermocouple calibrated against the melting point of gold, and located at less than 1 cm from the sample. As the temperature gradient was $\approx 0.5^\circ\text{C}/\text{cm}$ in the hot zone of the furnace and the charges were only a few mm long, the temperature variations within the experimental charges were negligible. Run durations ranged from 20 min to 496 h. At the end of the experiments, an electric current was passed through the platinum wire holding the capsule, the wire melted, and the capsule dropped into a recipient filled with cold water.

Analytical techniques

After the quench, some fragments of the sample were mounted in epoxy, ground and polished with 6, 3 and 1/4 μm diamond suspensions. Compositions of experimental glasses and plagioclases were determined with a Cameca SX100 electron microprobe (see Tables 2, 3 for analytical conditions). For textural analysis, we acquired back-scattered electron (BSE) images of the polished samples using a Cambridge Stereoscan S360 scanning electron microscope. The number of pixels per image was equal to 768 \times 574. Magnification was changed as a function of the grain size of the investigated sample so that the mean number of pixels per grain was similar in all the experiments ($\approx 1,100$ in the olivine experiments; ≈ 600 in the plagioclase experiments). Binary images were generated from the BSE images using MICROM-ORPH 1.3, an image analysis software developed by the Centre de Morphologie Mathématique, Ecole des Mines de Paris. On an average, we measured 350 grain sections per sample in the olivine experiments, and 230 in the plagioclase experiments. For each grain section, the two-dimensional (2D) size was taken as the diameter of the disc with the same area. Grains intersecting the edges of

the binary images were discarded. The 2D CSDs were corrected to compensate for the greater likelihood of large grains to intersect edges (see p. 249 in Russ and Dehoff 2000). The error on the 2D mean grain sizes (Table 1) comprised two components:

1. the analytical error on grain size measurements. Due to the intrinsic resolution of the BSE signal, the interface between a grain and the surrounding glass in a BSE image has a finite thickness of a few pixels. In Fig. 2d, for instance, the olivine grains and the glass have grey levels equal to ≈ 60 and 110, respectively, but they are separated by a 1- to 2-pixel thick transition zone with intermediate grey levels. Accordingly, we estimate that an analytical error on grain size of up to ± 2 pixels can arise depending on where the crystal-glass interface is placed in the transition zone.
2. the standard error of the mean value of the grain size distribution. As we are dealing with large populations of grain sizes ($N > 50$ –100, where N is the number of grains measured per sample), the confidence interval of the 2D mean grain size at the 95% confidence level can be approximated by $\bar{d} \pm 2s/\sqrt{N}$, where s is the standard deviation of the grain size distribution (Green and Margerison 1978).

The 2D CSDs were converted to three-dimensional (3D) CSDs to estimate the 3D mean grain size and the number of grains per unit volume (Table 1). In the olivine experiments, we assumed a spherical grain shape and we applied Saltykov corrections to the 2D CSDs (Saltykov 1967). In the plagioclase experiments, grain shape was assumed to be a rectangular parallelepiped, and we used the program ‘‘CSD Corrections’’ (Higgins 2000) to estimate the 3D mean grain size and the number of grains per unit volume. Because the Saltykov and Higgins procedures can lead to overcorrections and increase data dispersion, the CSDs shown in this paper are 2D CSDs and we plot both the 2D and 3D data in the grain size versus time diagrams.

Experimental results

Parageneses and phase compositions

Olivine series

The paragenesis in the olivine experiments is liquid + forsterite (+ air bubbles inherited from initial porosity; Fig. 2a–d). The concentrations of MgO and Al₂O₃ in the liquid phase are plotted as a function of run duration in Fig. 3a. They do not evolve with time, implying that no global crystallisation or dissolution of forsterite occurred after 20 min (the duration of the shortest experiment): the only process in operation in these experiments was Ostwald ripening. As expected, the experimental glasses are enriched in MgO and slightly depleted in Al₂O₃ compared to glass CMAS2

Fig. 2 a–h BSE microphotographs of polished sections of the olivine series (**a**, $t = 20$ min; **b**, $t = 15.4$ h; **c**, $t = 161.8$ h; **d**, $t = 496.4$ h), and of the plagioclase series (**e**, $t = 1$ h; **f**, $t = 9.6$ h; **g**, $t = 75$ h; **h**, $t = 336$ h). A few large air bubbles (*white arrows*) are visible in **a** and **d**, in addition to olivine (*dark grey*) and glass (*light grey*). The large plagioclase crystals in the long duration experiments (**g**, **h**) are commonly broken (the microcracks presumably developed during quench or sample preparation). *Scale bars*: 50 μm in **a–d**; 20 μm in **e–h**

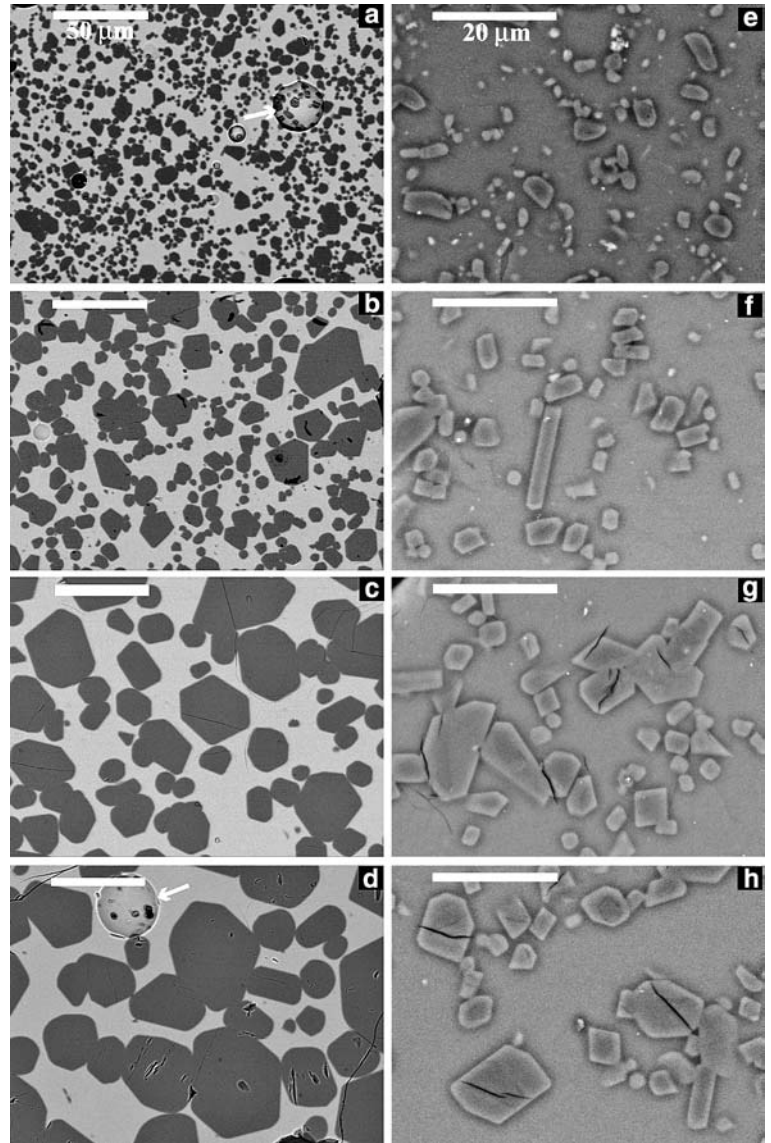


(Fig. 3a; Table 2): this is due to the fact that the run temperature was slightly larger than the liquidus temperature of glass CMAS2, resulting in the dissolution of some olivine (and all traces of enstatite in the olivine powder) within the first 20 min of the experiments.

Plagioclase series

The paragenesis in the plagioclase experiments is plagioclase + liquid (Fig. 2e–h); some air bubbles are also present. We did not detect any noticeable variation in the compositions of plagioclase and glass with time (Table 3). For instance, the Al_2O_3 concentrations in plagioclase and glass are nearly constant with time and very close to the initial values (Fig. 3b); plagioclase is just slightly more calcic than the starting plagioclase (An_{65} vs An_{64}). Accordingly, the natural labradorite used as starting plagioclase was in near-equilibrium with composition CMASN at 1 atm–1,250°C. Also, the FeO

content in glass is equal to 0.3 wt% in all the experiments, implying that the impurities in the plagioclase powder (magnetite, amphibole, etc.) were dissolved into the liquid in less than 1 h (the duration of the shortest experiment).

Textures

Textures in the plagioclase experiments were easily measurable due to the high volume fraction of the liquid phase (Fig. 2e–h). The samples were homogeneous and we did not observe anomalously large pools of liquid or plagioclase-rich domains (cumulates). Thus, we conclude that the textures were not affected by crystal settling or thermal migration (dissolution in the hot zone and precipitation in the cold zone of a thermal gradient; Walker et al. 1988), even in the longest plagioclase experiments.

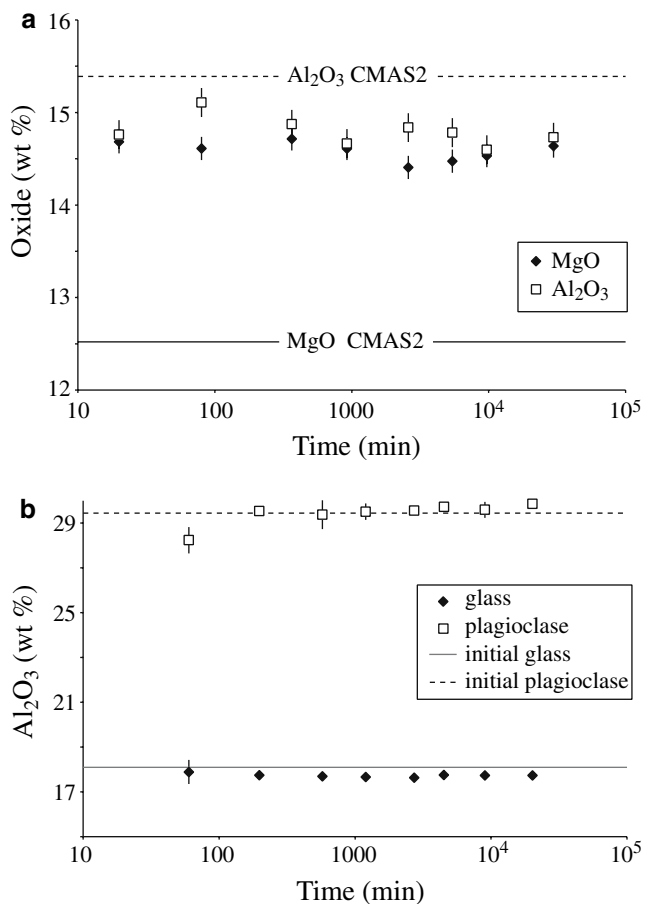


Fig. 3 **a** MgO and Al₂O₃ concentrations in glasses of the olivine experiments as a function of run duration; the concentrations in starting glass CMAS2 are shown for comparison. **b** Al₂O₃ concentrations in glasses and crystals of the plagioclase experiments as a function of run duration; the concentrations in starting glass CMASN and starting plagioclase are indicated

A few large pools of liquid were observed in some olivine experiments, often localized around large air bubbles (Fig. 4). An origin by crystal settling can be eliminated because the liquid pool in Fig. 4 is located at the bottom of the capsule, not at the top, and because we never observed olivine cumulates. An origin by thermal migration is unlikely because of the extremely low thermal gradient in our experiments: 0.5°C/cm. In their thermal migration experiments, Walker et al. (1988) observed major internal differentiations in the olivine-komatiite system, but for thermal gradients of ≈20–30°C/cm and typical run temperatures ≥1,400°C. Another argument against thermal migration is that the size of liquid pools does not increase with time: for instance, the large pool of liquid illustrated in Fig. 4 is from an intermediate duration experiment.

We believe that the large liquid pools in the olivine experiments resulted from some kind of filter-pressing occurring at the end of the experiments, during the few seconds in which the air bubbles were rapidly shrinking with decreasing temperature and the liquid was still above its glass transition temperature. As the volume

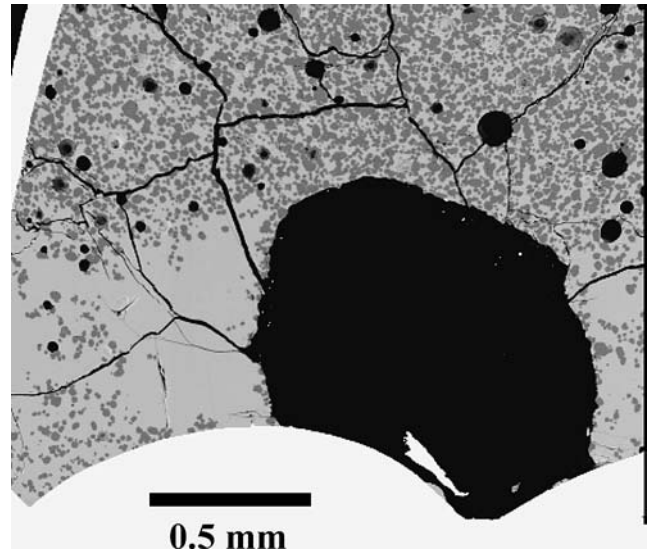


Fig. 4 A large air bubble surrounded by liquid pools at the bottom of the platinum capsule (white) in the olivine experiment Ol#6 ($t=90.4$ h); see text for explanation

fraction of crystals was large (≈50 vol.%; Table 1), they formed a relatively rigid framework unable to follow the rapidly retracting bubble interfaces: in this context, only the liquid could flow fast enough, leading to the formation of large pools surrounding the deflated bubbles.

Grain shape

Forsterite crystals are equant and show planar facets and rounded edges (e.g., Fig. 2c–d). This near-equilibrium crystal shape developed rapidly at the beginning of the experiments, and was already established in the 80-min run. On the basis of the equant shape of grain sections in the olivine experiments, a spherical shape was assumed for forsterite in the stereological corrections.

Plagioclase crystals are more elongated than forsterite crystals. They show planar facets and sharp edges; some edges may be slightly rounded, but with a radius of curvature much smaller than for forsterite and barely distinguishable in Fig. 2e–h. Because many grain sections were nearly parallelograms, a good approximation for the 3D shape of plagioclase grains is a rectangular parallelepiped. Following Higgins (1994), the relative lengths of the short, intermediate and long axes of the parallelepipeds were estimated by measuring the length and width of 400 grain sections in run Pl#3: these relative lengths are equal to 1, 2, and 4, respectively. The plagioclase grains developed their polyhedral morphology in a few hours (see, for instance, Fig. 2f). This fast transformation may be attributed to the very fine grain size of the starting powder.

Mean grain size

In both series, we observed an increase of the mean grain size with time, as a result of Ostwald ripening: the 3D

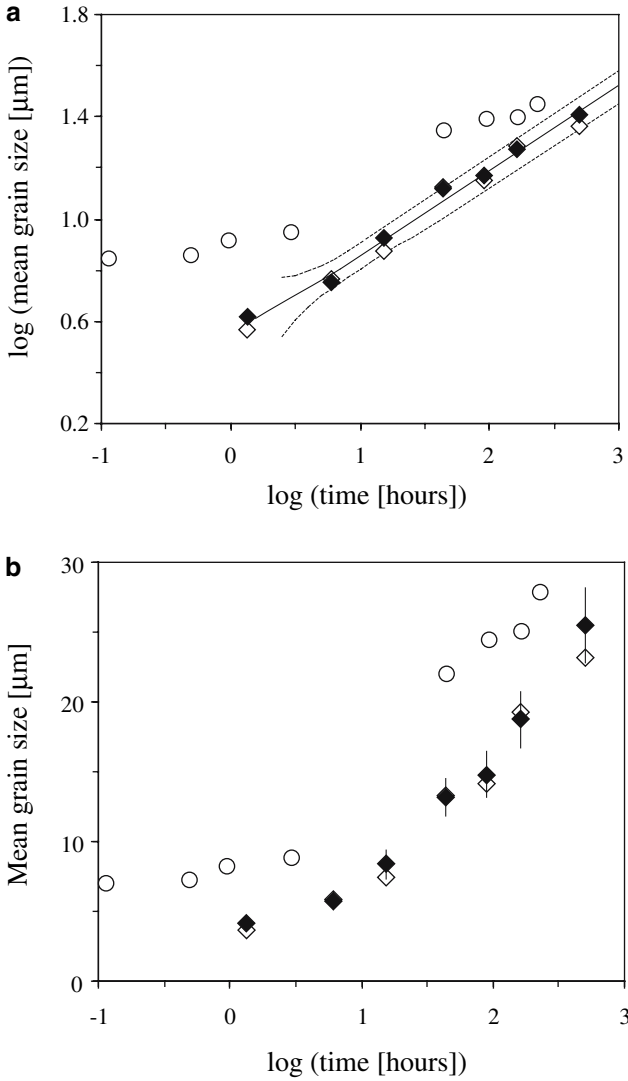


Fig. 5 a, b Mean grain sizes in the olivine series plotted as a function of run duration (solid diamonds: 2D mean sizes; empty diamonds: 3D mean sizes); the experimental data of Park and Hanson (1999), in the forsterite-basalt system at 1 atm–1,275°C, are shown for comparison (empty circles). **a** Logarithm of the mean grain size versus logarithm of time: in this plot, the data are best fitted by straight lines (not shown) with slopes equal to 0.32 for 2D mean grain sizes (correlation coefficient $R^2=0.989$) and 0.33 for 3D grain sizes ($R^2=0.982$). The solid line corresponds to the straight line best fitting the experimental data in the cube of grain size versus time diagram: $\bar{d}^3 = 36.1 t + 13.4$; the error on the calculated mean grain size is shown by the dashed lines (see Table 7 for details). **b** Mean grain sizes plotted as a function of the logarithm of time; the errors on the 2D mean grain sizes are shown (the error bars are not shown in **a** because they are nearly equal to symbol size)

mean grain size increases from $\approx 3 \mu\text{m}$ to $23.2 \mu\text{m}$ in 496 h in the olivine series (Fig. 1a–d), and from $\approx 3 \mu\text{m}$ to $8.7 \mu\text{m}$ only in 336 h in the plagioclase series (Fig. 1e–h). In a $\log(\bar{d})$ versus $\log(t)$ diagram, a data set following Eq. 8 should yield a straight line with a slope equal to $1/n$ (provided $\bar{d} \gg \bar{d}_0$). In such a diagram, the 2D mean grain sizes of olivine plot as a straight line with

a slope of 0.32 and a correlation coefficient $R^2=0.989$ (0.33 and 0.982, respectively, for the 3D mean grain sizes; Fig. 5a). These slopes correspond to an exponent $n=3.0$ ($-0/+0.1$), as predicted for Ostwald ripening controlled either by diffusion in the liquid or by the operation of screw dislocations at solid-liquid interfaces. For comparison, we also plotted the olivine data in a \bar{d} versus $\log(t)$ diagram (Fig. 5b). In the case of a control by surface nucleation, mean grain sizes should plot as a straight line in such a diagram (provided the term t/τ in Eq. 10 is large enough). Figure 5b indicates that Ostwald ripening in the olivine-basalt system is not controlled by surface nucleation.

The mean grain sizes of plagioclase are plotted in a $\log(\bar{d})$ versus $\log(t)$ diagram and in a \bar{d} versus $\log(t)$ diagram (Fig. 6a and b, respectively). Figure 6a shows that Eq. 8 may provide a good fit to the plagioclase data but only if the exponent n is set to ≈ 7 . This exponent is, however, much larger than the theoretical values predicted for Ostwald ripening controlled by diffusion ($n=3$), spiral growth ($n=3$), or continuous growth ($n=2$). A control by surface nucleation seems more likely because the plagioclase mean grain sizes plot as straight lines in the \bar{d} versus $\log(t)$ diagram (Fig. 6b). Whatever the rate-limiting mechanism, Fig. 6 shows that 2D mean grain sizes are more suitable for the interpretation of Ostwald ripening experiments than 3D mean grain sizes: indeed, both sets of data obey similar kinetic laws but the dispersion of the former is much smaller.

Crystal size distributions

The 2D CSDs measured in the olivine and plagioclase experiments are reported in Tables 4 and 5, and illustrated in Fig. 7 (each distribution was normalised by dividing all grain sizes by the mean grain size; cf. Table 1). In a suspension undergoing Ostwald ripening, the normalised CSD is expected to evolve toward a stationary shape, which depends on the mechanism controlling the kinetics. Therefore, it is important to study the evolution of CSDs with time in our experiments. Three CSDs from the olivine series are shown in Fig. 7a: they are all very similar, and there is only little evolution between 80 min and 496 h. In the plagioclase series (Fig. 7b), we observe a slight evolution of CSDs between 1 h and 20 h, the frequencies of normalised grain sizes in classes [0.66–1.00] and [1.00–1.33] increasing at the expense of class [0.33–0.66]. Then, the distribution seems to stabilise: the CSDs at 20 h and 336 h are nearly identical.

Number of grains

The number of grains per unit volume, N_v , is plotted as a function of time in Fig. 8. It decreased by more than two orders of magnitude over 496 h in the olivine series, and by more than a factor 20 over 336 h in the plagioclase

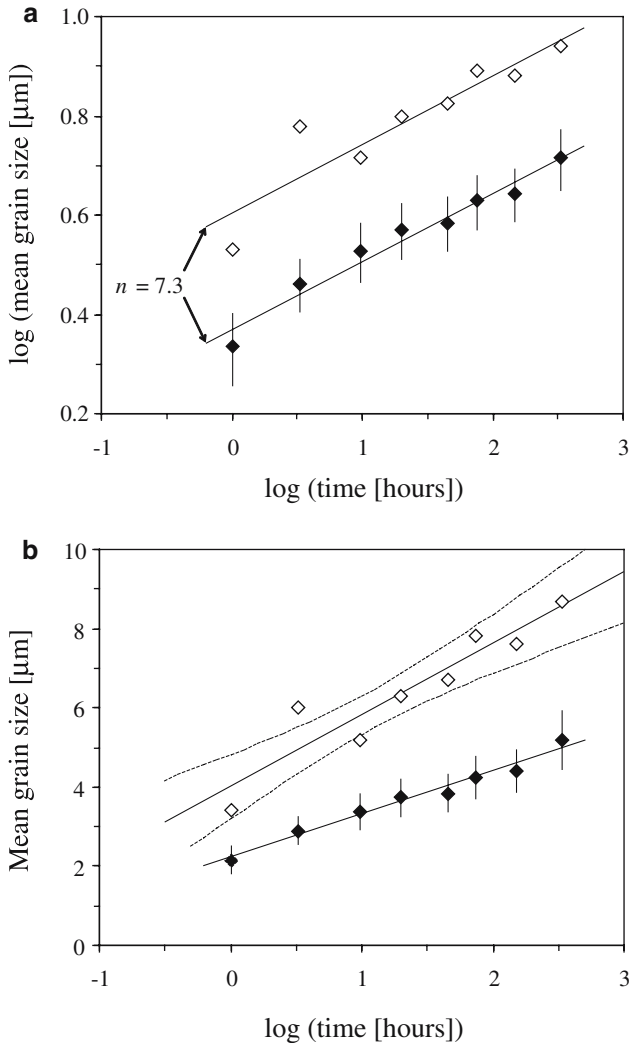


Fig. 6 a-b Mean grain sizes in the plagioclase series plotted as a function of run duration (*solid diamonds*: 2D mean sizes; *empty diamonds*: 3D mean sizes). **a** Logarithm of the mean grain size versus logarithm of time. The data are best fitted by *straight lines* with slopes equal to 0.1369 for 2D mean grain sizes ($R^2=0.965$) and 0.1378 for 3D grain sizes ($R^2=0.841$), yielding a value $n=7.3$ for the exponent in equation [8]. **b** Mean grain sizes plotted as a function of the logarithm of time. The correlation coefficient of the best fit line for 2D mean grain sizes is equal to 0.977. The *solid line* fitted to the 3D mean grain sizes is the best fit line used for extrapolation to long durations: $\bar{d} = 1.806 \log(t) + 4.0$; the *dashed lines* are displaced vertically from the best fit line by \pm two standard deviations of the calculated mean grain size (see Table 7 for details)

series. In both cases, N_v is linearly related to time at the power α :

$$N_v \propto t^\alpha \quad (11)$$

with $\alpha = -0.87$ in the olivine series, and $\alpha = -0.44$ in the plagioclase series. The value $\alpha = -0.87$ in the olivine series is close to the theoretical value for grain coarsening in $t^{1/3}$: $\alpha = -1$. Assuming for simplicity that the olivine grains are equal-sized spheres of diameter d , then the volume fraction of olivine grains is equal to $(N_v \times \pi d^3)/6$. Accordingly, if d increases as $t^{1/3}$, then N_v must

decrease as t^{-1} because the volume of the solid phase is essentially constant during Ostwald ripening.

Discussion

Identification of the mechanisms controlling Ostwald ripening in the experiments

Plagioclase series

The plagioclase data are well fitted by Eq. 10, but not by Eq. 8 with $n=2$ or 3 (Fig. 6). Accordingly, Ostwald ripening in the plagioclase experiments seems to be controlled by a surface nucleation process at the crystal/liquid interface, with the mean grain size increasing as $\log(t)$. There is, however, one major difficulty in the interpretation of Ostwald ripening experiments from the grain size versus time relationships: the theoretical laws [8–10] correspond to stationary regimes that may not be established in short duration experiments. To illustrate this difficulty, we plotted our plagioclase data in a \bar{d}^3 versus t diagram (Fig. 9a). From this diagram, we could conclude that, after a transient regime lasting ≈ 15 h, a stationary regime where \bar{d}^3 was proportional to t was established, with coarsening controlled either by diffusion in the liquid or by a screw dislocation mechanism. If we assume a diffusion control, we can use Eq. 9 to compute the effective diffusion coefficient D from the slope of the straight line best fitting the 3D mean grain sizes in a \bar{d}^3 versus t diagram (for $t \geq 20$ h): $1.2 \mu\text{m}^3/\text{h}$. Setting $T=1523$ K, $V_\beta=0.000101 \text{ m}^3/\text{mol}$, $\sigma_{\alpha\beta}=0.5 \text{ J}/\text{m}^2$, $c_0=0.6$, we find $D=2 \times 10^{-14} \text{ m}^2/\text{s}$. This estimate is lower than the value expected for the slowest diffusing species in an andesitic melt at $1,250^\circ\text{C}$ (supposedly SiO_2 , $D \approx 10^{-12} \text{ m}^2/\text{s}$; Zhang et al. 1989): the diffusion rate in the plagioclase experiments is too fast to control the kinetics of Ostwald ripening.

At present, we cannot definitely exclude the hypothesis of a screw dislocation control. We emphasize, however, that this hypothesis is based on the artificial splitting of the experimental data in two regimes (Fig. 9a), whereas Fig. 6b suggests a consistent set of data. Also we did not find in the literature evidence indicating that plagioclase grows by a screw dislocation mechanism at low ΔT . Watanabe and Kitamura (1992) studied the growth mechanisms of labradorite in a basaltic melt, but their data do not allow to discriminate between spiral growth and surface nucleation as the dominant growth mechanism at $\Delta T \leq 30^\circ\text{C}$. In addition, Kirkpatrick et al. (1976) showed that anorthite grows by surface nucleation at small undercoolings. Accordingly, we shall consider in the following that Ostwald ripening in the plagioclase experiments was controlled by a surface nucleation mechanism at solid-liquid interfaces. The same conclusion was drawn for Ostwald ripening in the quartz-granite system (Cabane et al. 2001).

Table 4 Normalised crystal size distributions (2D) in the olivine experiments

	OI#8	OI#11	OI#9 ^a	OI#5	OI#6	OI#7	OI#10
1/3	0.041	0.013	0.067	0.037	0.051	0.044	0.058
2/3	0.252	0.223	0.248	0.193	0.203	0.178	0.214
3/3	0.327	0.347	0.287	0.347	0.340	0.360	0.328
4/3	0.183	0.214	0.186	0.215	0.220	0.225	0.177
5/3	0.084	0.111	0.101	0.108	0.093	0.098	0.116
6/3	0.046	0.048	0.050	0.067	0.038	0.060	0.057
7/3	0.013	0.030	0.030	0.022	0.036	0.022	0.034
8/3	0.028	0.007	0.014	0.007	0.008	0.008	0.012
9/3	0.015	0.007	0.006	0.004	0.008	0.004	0.000
10/3	0.008	0.000	0.000	0.000	0.000	0.000	0.004
11/3	0.004	0.000	0.003	0.000	0.000	0.000	0.000
12/3	0.000	0.000	0.000	0.000	0.005	0.000	0.000
δ_{\max}	3.5	2.9	5.5	2.9	4.0	2.8	3.1
σ	0.59	0.47	0.63	0.47	0.53	0.47	0.52
ξ	1.54	1.09	2.20	0.81	1.48	0.85	0.94

To calculate the CSDs, we measured an average of 350 grain sections per sample (see Table 1). The actual size of a section was taken as the diameter of the disc with the same area. We normalised the data by dividing all sizes by the mean size of the grain sections. For each sample, the Table gives the relative frequencies of olivine sections in normalised size intervals equal to 1/3; the number in the first column is the upper limit of the size interval: in sample OI#8,

for instance, 18.3% of the grain sections have a size comprised between 1 and 4/3. The maximum normalised grain size, δ_{\max} , the standard deviation, σ , and the skewness, $\xi = (\text{mean} - \text{mode})/\sigma$, of the CSD are given in the last three rows

^aIn addition, sample OI#9 contains 0.4% grain sections with an area in the range 4 to 13/3, and 0.4% with an area in the range 5 to 16/3

Olivine series

The grain size data in the olivine series follow a kinetic law in $t^{1/3}$ (Fig. 5a), and are therefore in agreement with either a control by diffusion in the liquid or by a screw dislocation mechanism at interfaces. The slope of the straight line best fitting the olivine data in the \bar{d}^3 versus t diagram is equal to $36.1 \mu\text{m}^3/\text{h}$ (see below). If we assume a diffusion control, this slope implies an effective diffusion coefficient for Ostwald ripening equal to $D \approx 3 \times 10^{-12} \text{m}^2/\text{s}$ (from Eq. 9, with $T = 1,573 \text{K}$, $V_{\beta} = 0.000044 \text{m}^3/\text{mol}$, $\sigma_{\alpha\beta} = 0.5 \text{J}/\text{m}^2$, $c_0 = 0.26$). This estimate is lower than the diffusivity of Si in a basaltic

melt ($D \approx 10^{-11} \text{m}^2/\text{s}$; Leshner et al. 1996; LaTourette et al. 1996), but by less than one order of magnitude: this difference is not sufficient to eliminate definitively the hypothesis of a diffusion control in the olivine experiments. The shape of the experimental CSDs provides, however, another argument against a diffusion control, as discussed below.

The exact shape of stationary CSDs in diffusion controlled Ostwald ripening depends on the volume fraction of the solid phase and on the theory taken in consideration (Lifshitz and Slyozov 1961; Ardell 1972; Brailsford and Wynblatt 1979; Marqusee and Ross

Table 5 Normalised crystal size distributions (2D) in the plagioclase experiments

	PI#8	PI#7	PI#5	PI#2	PI#6	PI#9	PI#4	PI#3
1/3	0.005	0.000	0.034	0.000	0.000	0.000	0.000	0.000
2/3	0.261	0.141	0.131	0.185	0.169	0.106	0.127	0.177
3/3	0.359	0.406	0.432	0.458	0.438	0.498	0.495	0.429
4/3	0.178	0.276	0.228	0.223	0.242	0.260	0.243	0.229
5/3	0.107	0.140	0.062	0.069	0.082	0.067	0.071	0.092
6/3	0.050	0.021	0.080	0.039	0.041	0.040	0.030	0.045
7/3	0.017	0.011	0.025	0.005	0.007	0.025	0.020	0.020
8/3	0.018	0.006	0.009	0.005	0.018	0.004	0.000	0.003
9/3	0.006	0.000	0.000	0.005	0.004	0.000	0.015	0.003
10/3	0.000	0.000	0.000	0.006	0.000	0.000	0.000	0.003
11/3	0.000	0.000	0.000	0.006	0.000	0.000	0.000	0.000
δ_{\max}	3.0	2.5	2.7	3.7	2.9	2.6	3.0	3.3
σ	0.48	0.36	0.45	0.45	0.42	0.37	0.41	0.41
ξ	1.27	0.86	0.89	2.35	1.50	1.35	1.88	1.40

To calculate the plagioclase size distributions, we measured the size of ≈ 230 grain sections per sample (see Table 1). We used the same normalisation procedure as for the olivine CSDs (Table 4). For each sample, the Table gives the relative frequencies of plagioclase sections in normalised size intervals equal to 1/3; the number in the

first column is the upper limit of the size interval. The maximum normalised grain size, δ_{\max} , the standard deviation, σ , and the skewness, $\xi = (\text{mean} - \text{mode})/\sigma$, of the CSD are given in the last three rows

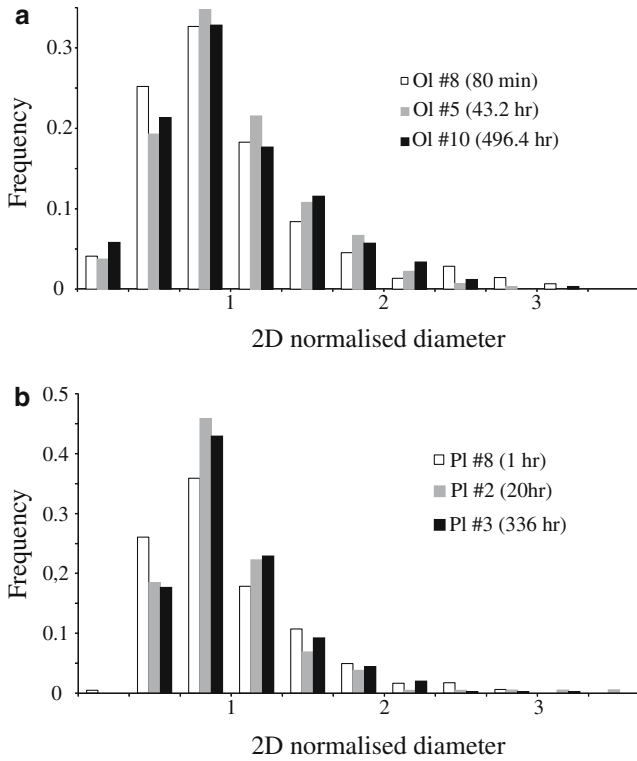


Fig. 7 a, b Normalised 2D crystal size distributions in the olivine series (a) and in the plagioclase series (b). Three CSDs are shown for each series; grain size classes are the same as in the first column of Tables 4, 5

1984; Dehoff 1991). The shape of all theoretical CSDs can, however, be considered as intermediate between two end-members: the first one corresponds to the normalised CSD predicted by LSW theory (Lifshitz and Slyozov 1961; Wagner 1961); the second end-member is

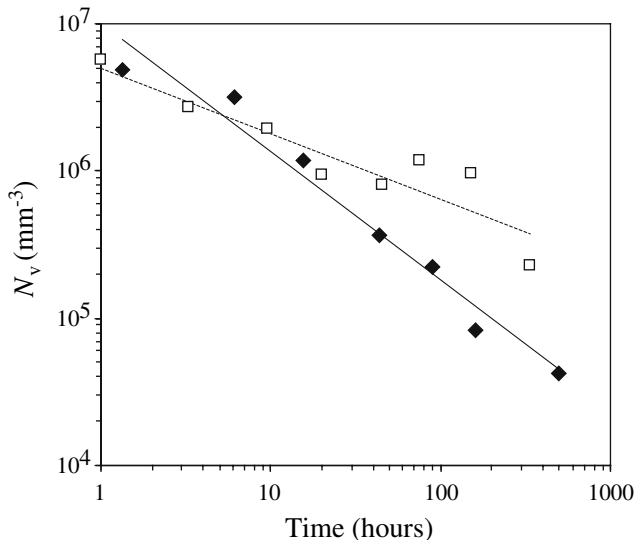


Fig. 8 Number of grains per unit volume, N_v (mm^{-3}), plotted as a function of run duration; the solid diamonds correspond to the olivine series, and the empty squares to the plagioclase series. The experimental data are fitted by power laws in time

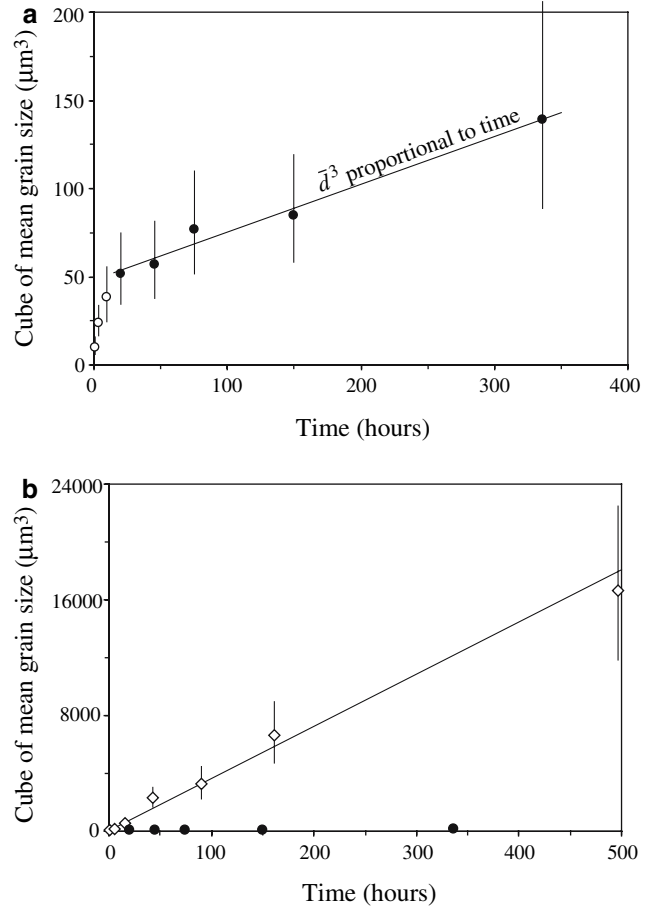


Fig. 9 a, b a Cube of the 2D mean grain size in the plagioclase experiments plotted as a function of run duration. In this type of projection, the data for durations $t \geq 20.0$ h (solid circles) can be fitted by a straight line; empty circles correspond to the short duration experiments ($t \leq 10$ h). b Cube of the 2D mean grain size in the olivine experiments (diamonds) plotted as a function of run duration; the solid line corresponds to the straight line best fitting the experimental data: $\bar{d}^3 = 36.1 \cdot t + 13.4$. Plagioclase mean grain sizes are shown for comparison (circles; grain sizes at $t \leq 10$ h not plotted for clarity)

the CSD predicted by the Communicating Neighbours theory (Dehoff 1991). The main features of these theoretical CSDs are summarized in Table 6. Clearly, the CSDs in the olivine experiments differ from those predicted for diffusion controlled Ostwald ripening (as the correction procedure used to convert measured CSDs into 3D CSDs increases data dispersion, we compare directly the 2D CSDs with apparent theoretical CSDs in a random section). First, the maximum normalised grain size in the experiments is equal to 3.5 on average (Table 4), whereas theories predict a maximum 2D grain size comprised between 1.8 and 2.6 (Table 6; maximum grain sizes in the experiments are conservative estimates, which should increase with increasing number of measurements). Second, diffusion controlled Ostwald ripening leads to negatively skewed normalised CSDs, whereas the CSDs measured in the olivine experiments are all positively skewed, with skewness ζ in the range 0.8 to 1.5 (Table 4).

Table 6 Maximum grain size, δ_{\max} , standard deviation, σ , and skewness, ξ , of normalised CSDs produced by Ostwald ripening (in the steady-state regime)

Theory ^a	2D/3D ^b	δ_{\max}	σ	ξ^c
Diffusion 1	3D	1.5	0.215	-0.920
	2D	1.849	0.344	-0.488
Diffusion 2	3D	2	0.314	-0.291
	2D	2.581	0.408	-0.074
Screw dislocations	3D	3	0.325	0.744
	2D	3.636	0.447	0.503

^a“Diffusion 1”, theoretical CSD predicted for diffusion-controlled Ostwald ripening by LSW theory (Lifshitz and Slyozov 1961; Wagner 1961). “Diffusion 2”, theoretical CSD predicted for diffusion-controlled Ostwald ripening by the Communicating Neighbours theory (Dehoff 1991). “Screw dislocations”, theoretical CSD in the case where Ostwald ripening is controlled by the operation of screw dislocations at solid-liquid interfaces (Cabane 2002)

^bThe rows labelled “3D” correspond to three-dimensional CSDs. To make the comparison between experiments and theory easier, the shape of apparent CSDs in a random section (rows labelled “2D”) was computed from the 3D CSDs. The stereological corrections needed to convert the 3D CSDs into 2D distributions were made assuming a spherical grain shape. All CSDs were normalised, as follows: the 3D CSDs were normalised to the 3D critical grain size; for 2D CSDs, the size of all grain sections was divided by the 2D mean grain size

^c $\xi = (\text{mean} - \text{mode})/\sigma$

The case of Ostwald ripening controlled by spiral growth has been considered empirically by Chai (1974), and theoretically by Kahlweit (1975), Ratke et al. (1995), and Cabane (2002). In this case, the normalised CSD is positively skewed, and the maximum 2D grain size is equal to 3.6 (Table 6). Accordingly, the main features of the olivine CSDs (positive skewness, large maximum grain size) are better reproduced by a model in which the kinetics of Ostwald ripening is controlled by screw dislocations. This conclusion was confirmed by numerical computations of grain coarsening in the olivine-basalt system (Cabane 2002). As predicted by analytical studies, both the diffusion model and the screw dislocation model reproduce nicely the kinetic law in $t^{1/3}$. However, only the screw dislocation model is able to reproduce the experimental CSDs, as illustrated in Fig. 10.

We did not find in the literature an independent proof of a screw dislocation mechanism for olivine growth at very small undercoolings. Jambon et al. (1992) measured olivine growth rates in a tholeiitic basalt, but they did not identify the growth mechanisms. There exists, however, at least one major mafic silicate whose dominant growth mechanism at small undercoolings is spiral growth: diopside (Kirkpatrick et al. 1976). In addition, computer simulations of crystal growth showed that at very low degrees of undercooling, layer growth in the presence of screw dislocations is much faster than by surface nucleation alone (Gilmer 1976). Accordingly, a screw dislocation mechanism could explain the much faster kinetics of Ostwald ripening in the olivine series, compared to the plagioclase series (Fig. 9b).

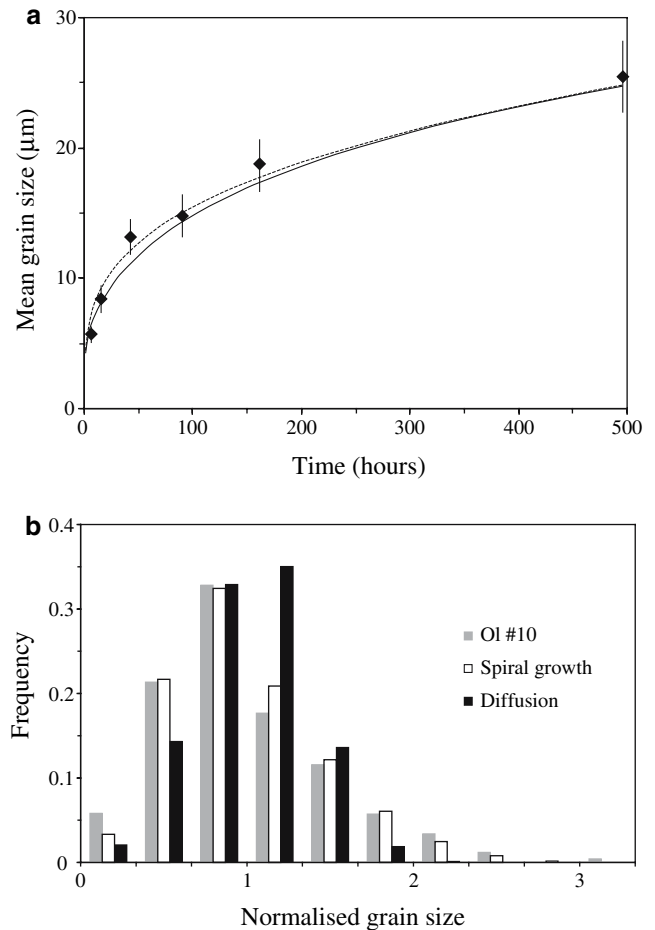


Fig. 10 a-b. Numerical simulation of Ostwald ripening in the olivine-basalt system (Cabane 2002). **a** Evolution of the 2D mean grain size with time for grain coarsening controlled by a screw dislocation mechanism (*continuous line*) or by diffusion in the liquid (*dashed line*); the mean grain sizes measured in the olivine series are shown by the *solid diamonds*. **b** Normalised 2D crystal size distributions at time $t = 496.4$ h (same grain size intervals as in Table 4): the CSDs computed for a screw dislocation control (*white*) and a diffusion control (*black*) are compared to the CSD measured in sample Ol#10 (*grey*)

Comparison with previous studies

The behaviour in our plagioclase series is very similar to that previously described for quartz in silicic melts (Cabane et al. 2001). First, Ostwald ripening of quartz was extremely sluggish: in a granitic liquid with 6 wt% dissolved water, at 1 GPa–900°C, the mean grain size of quartz increased from 2.8 μm to only 8.2 μm in 519 h. Second, grain sizes increased as $\log(t)$, indicating a kinetic control by surface nucleation.

Park and Hanson (1999) studied the coarsening of forsterite grains in a basaltic liquid at 1 atm–1,275°C. They observed a relatively fast increase of the mean grain size with time, from 7 μm to 28 μm in 9.8 days, in good agreement with our olivine series. Park and Hanson could not identify the rate-limiting process, but they only tried to fit their data with $t^{1/2}$ or $t^{1/3}$ laws. In a

$\log(\bar{d})$ versus $\log(t)$ diagram (Fig. 5), their data plot as a straight line with a more gentle slope than our data, and can be fitted by a power law with an exponent $n \approx 4.5$. Accordingly, grain coarsening in their experiments seems to follow a kinetic law intermediate between a power law in $t^{1/3}$ and a law in $\log(t)$. One difficulty with Park and Hanson's (1999) experiments is that they used a starting composition with only ≈ 10 vol.% olivine (by visual estimate) so that the crystals settled down and formed aggregates at the bottom of the charges in the long duration runs. As a consequence, some grain coalescence occurred in addition to Ostwald ripening, and could explain why it is not possible to fit the grain size data with either a $t^{1/3}$ or a $\log(t)$ law. Grain coalescence was presumably responsible for the development of grains exceeding $150 \mu\text{m}$ in the 9.8-day experiment: by comparison, the maximum grain size in our 20.7-day experiment is $\approx 75 \mu\text{m}$. Also, despite a slightly lower temperature ($1,275^\circ\text{C}$ vs $1,300^\circ\text{C}$), a linear fit to their data set in a \bar{d}^3 versus t diagram yields a slope equal to $99 \mu\text{m}^3/\text{h}$, which is three times larger than the ripening rate in our experiments $36 \mu\text{m}^3/\text{h}$.

The effect of thermal cycling on the kinetics of Ostwald ripening

Temperature in 1-atm furnaces is subject to periodic variations of a fraction of a degree that could have a non negligible effect on the kinetics of Ostwald ripening. A rise of $\approx 0.5^\circ\text{C}$ above the mean temperature could indeed lead to the complete dissolution of the smallest grains and result in a non trivial increase of the mean grain size. In our furnaces, the amplitude of thermal fluctuations is $\pm 0.3^\circ\text{C}$, with periods ranging from a few tens of seconds to a few minutes. We discuss below the effects of thermal cycling on Ostwald ripening and come to the conclusion that these effects are more likely to be of second order in our experiments.

Let us consider a system similar to the plagioclase-andesite experiments, with $T = 1,250^\circ\text{C}$, $c_0 = 0.6$, $dc_0/dT = 0.0015^\circ\text{C}^{-1}$ (from the slope of the plagioclase saturation curve in the diopside-anorthite binary; Weill et al. 1980), and a crystal fraction of 20 wt %. We emphasize that, in such a system, fluctuations of $\pm 0.5^\circ\text{C}$ correspond to very small variations of the equilibrium crystal fraction: $\pm 0.1\text{wt}\%$. At the time t under consideration, the critical grain size $2r^*$ is supposed to be equal to $10 \mu\text{m}$, a value which corresponds to $c_1 = 0.60096$ (c_1 is the mass fraction of plagioclase dissolved in the liquid; as we are dealing with very small variations of concentrations, we directly use the mass fractions instead of the mole fractions in Eq. 5); the mean grain size is nearly equal to the critical grain size, as is always true for Ostwald ripening in the stationary regime, whatever be the rate-limiting mechanism. At this point, we assume that T increases suddenly by 0.5°C . This fluctuation produces changes in c_0 and r_0 (see Eq. 5), at constant c_1 ; as a result, r^* increases from $5 \mu\text{m}$ to $22.8 \mu\text{m}$, that is, all

the grains with a radius in the range $5\text{--}22.8 \mu\text{m}$ switch from a growth regime to a dissolution regime. The increase in r^* is temporary: with time, a small quantity of plagioclase will be dissolved into the liquid, c_1 will increase (at constant c_0 and r_0), and r^* will decrease to a value close to the mean grain radius: $\approx 5 \mu\text{m}$. The time it will take for the system to relax depends on the diffusion coefficient and on the number density of grains, which controls the average distance between two grains. For $N_v \approx 10^6 \text{mm}^{-3}$ (Table 1), the average distance between two grains is $< 10 \mu\text{m}$ and the time scale of relaxation is of the order of 10 s.

The degrees of undercooling just after the temperature step at 1250.5°C (when $r^* = 22.8 \mu\text{m}$) are plotted as a function of grain size in Figure 1: they are systematically lower by $0.3\text{--}0.4^\circ\text{C}$ than the ΔT_s at $1,250^\circ\text{C}$. The relative changes in ΔT are, however, much more important for large grains than for small ones: (1) ΔT drops from 0.34°C to 0 (that is, the growth rate drops to zero) for grain sizes equal to $45.6 \mu\text{m}$, and from 0 to -0.34°C for grain sizes equal to $10 \mu\text{m}$; and (2) for grains of $0.1 \mu\text{m}$, ΔT decreases from -43.6°C to -43.9°C . Whatever the dissolution mechanism, this 0.6 % decrease in ΔT cannot lead to a significant increase of the dissolution rate of small grains. Accordingly, thermal cycling will primarily affect large grains not small ones, and, for a given grain size, the increased dissolution rates (or decreased growth rates) at 1250.5°C will be balanced by increased growth rates (or decreased dissolution rates) at 1249.5°C , as displayed in Fig. 1. These observations coupled with the very small variations of the crystal fraction of plagioclase induced by 0.5°C fluctuations suggest that the kinetics of Ostwald ripening in our experiments was not significantly affected by thermal cycling.

Geological implications

Importance of Ostwald ripening in geological systems

Extrapolations to geological time scales In order to estimate the effects of Ostwald ripening on the grain size of olivine and plagioclase in magmatic systems, we extrapolated our results to time scales up to 10^5 years. We used the method of least squares to fit straight lines to the experimental data, taking the errors on grain size into account as described in Green and Margerison (1978). For olivine, a straight line was fitted to the data points in the \bar{d}^3 versus t diagram. The best fit line is: $\bar{d}^3 = 36.1 t + 13.4$, with t in hours and \bar{d} in μm (Fig. 9b); the value of the intercept, 13.4, corresponds to an initial mean grain size $\bar{d}_0 = 2.4 \mu\text{m}$. For plagioclase, a straight line was fitted to the data points in the \bar{d} versus $\log(t)$ diagram. The best fit line is: $\bar{d} = 1.806 \log(t) + 4.0$, where t is in hours and \bar{d} in μm (Fig. 6b). These different laws lead to dramatically different evolutions (Table 7; Fig. 9b). For plagioclase, the mean grain size increases from an initial value of $\approx 4 \mu\text{m}$ to $11 \mu\text{m}$ in 1 year, and

Table 7 Mean grain sizes extrapolated from our experimental data to times t equal to 1, 10, 10^3 , and 10^5 years

Duration (Years)	Mean grain size (μm)	
	Olivine ^a	Plagioclase ^b
1	68 ± 10	11 ± 2
10	147 ± 21	13 ± 2
1,000	680 ± 100	17 ± 4
10^5	3160 ± 460	20 ± 5

^aFor olivine, we used the method of least squares to fit a straight line to the experimental data in the \bar{d}^3 versus t diagram. The best fit line is: $\bar{d}^3 = 36.1 t + 13.4$, with t in hours and \bar{d} in μm . The correlation coefficient R^2 is equal to 0.953, and the variance s^2 of \bar{d}^3 is given by: $s^2 = 45.412 (t - 2.56)^2 + 956.7$. Errors on grain size were taken into account as described in Green and Margerison (1978) and were adjusted so that all experimental data fall within ± 2 s of the best fit line (Fig. 5a).

^bFor plagioclase, a straight line was fitted to the experimental data in the \bar{d} versus $\log(t)$ diagram. The best fit line is: $\bar{d} = 1.806 \log(t) + 4.0$, where t is in hours and \bar{d} in μm . The correlation coefficient R^2 is equal to 0.838, and the variance of \bar{d} to $0.09 [\log(t) - 1.1]^2 + 0.06$. In the calculations, errors on 3D mean grain sizes were adjusted so that experimental data fall within ± 2 s of the best fit line (except the outlier at $t = 3.3$ h; Fig. 6b).

then to only 20 μm in 10^5 years. For olivine, the mean grain size increases from an initial value of 2–3 μm to 68 μm in 1 year, and to 680 μm in 10^3 years; a mean grain size of ≈ 3 mm is reached in 10^5 years.

The influence of Ostwald ripening on the dynamics of magmatic processes One of the motivation for this study was to evaluate the effect of Ostwald ripening on the dynamics of magmatic processes, noting that an increase by a factor f of the mean grain size will increase by a factor f^2 the settling velocity of crystals or the permeability of a partially molten rock. In the case of plagioclase, Ostwald ripening is very sluggish, and is only efficient for mean grain sizes of a few microns to ≈ 20 μm . The size of plagioclase crystals in magmatic systems is usually ≥ 100 μm , and up to a few cm: in such systems, Ostwald ripening cannot lead to a measurable increase of the mean grain size even for a time scale of 10^5 years, and therefore cannot accelerate processes such as settling or flotation of plagioclase crystals.

Ostwald ripening is much faster in the olivine-basalt system (see also, Park and Hanson 1999), but its effect on crystal settling remains presumably of second order. For instance, it would take about 20 years for an olivine grain of 500 μm to settle at the bottom of a 1 km thick magma chamber: in 20 years, the effect of Ostwald ripening would be to increase the grain diameter by only 7 μm . There are, however, two magmatic processes whose dynamics may be influenced by grain coarsening: compaction of olivine-rich cumulates and melt extraction from partially molten peridotites (note that grain coarsening in a partially molten rock or in a crystal mush is driven by interfacial energy minimization, but it is not strictly Ostwald ripening because grain growth results in a large part from grain boundary migration,

not from a solution/precipitation process). Our experiments suggest that an increase of the mean grain size of olivine by a factor 10 or more is attainable in these situations because the time scale may exceed 10^3 – 10^5 years (Table 7).

The effect of Ostwald ripening on the CSDs of magmatic rocks Our experiments on plagioclase, olivine, and quartz show that Ostwald ripening cannot directly produce magmatic textures with mean grain sizes of hundreds of μm or a few millimetres (except may be in some cases for olivine). Indirectly, however, Ostwald ripening may have an important effect on igneous textures because it reduces the number of crystals per unit volume: when the mean grain size is multiplied by a factor f , the number of grains is divided by f^3 , roughly. The situation we envision is as follows: a large volume of silicate liquid is slowly cooling, and once a sufficient degree of undercooling is reached, a nucleation event is triggered; subsequent crystal growth brings the system back to near-equilibrium, with a small degree of undercooling ($< 1^\circ$). At this stage, the system is crowded with micron-sized crystals, and is in an ideal state for the operation of Ostwald ripening: in one year, the number of grains will decrease by a factor 20 in the case of plagioclase and by four orders of magnitude in the case of forsterite (we assumed an initial mean size of 2.4 μm for olivine and 4.0 μm for plagioclase, and we used the extrapolations in Table 7).

Assuming a constant growth rate and a nucleation rate increasing exponentially with time, Marsh (1988) showed that closed-system crystallisation should produce straight CSDs in a plot of $\ln[n_v(r)]$ versus r , where $n_v(r)$ is the population density (in m^{-4} ; $n_v(r) \times dr$ is the number of grains with a radius in the range r to $r + dr$, per unit volume). The CSDs of many igneous rocks are, however, convex upwards, and show a deficiency of small grains as compared to the predicted logarithmic-linear correlation (Higgins 1998; Marsh 1998; Bindeman 2003). Ostwald ripening could explain this feature, but only if the deficient size intervals are less than a few tens of μm for quartz and plagioclase, and less than about 100 μm in the case of olivine. By comparison, grain sizes up to a few hundreds of μm to a few mm are deficient in natural CSDs: such deficiencies cannot be solely explained by Ostwald ripening, but could result from a combination of Ostwald ripening followed by crystal growth (with no additional nucleation).

Growth mechanisms of silicates at very low degrees of undercooling

If we except the case of crystals growing near chamber walls, the degrees of undercooling governing the crystallisation of large magmatic bodies may be very low (< 1 to 5°C ; e.g., Brandeis et al. 1984; Hort and Spohn 1991; Worster et al. 1990). They are therefore very difficult to reproduce in the laboratory using classical

crystal growth techniques (e.g., Kirkpatrick 1981; Jambon et al. 1992). Ostwald ripening involves degrees of undercooling that are essentially $< 1^{\circ}\text{C}$ (Fig. 1), close to those prevailing in large magma chambers. Thus the mechanisms and rates of crystal growth at $\Delta T \rightarrow 0^{\circ}\text{C}$ could be constrained by studying the kinetics of Ostwald ripening in silicate systems (provided the kinetics is not diffusion-controlled).

For plagioclase in an andesitic liquid (this study) and for quartz in a granitic liquid (Cabane et al. 2001), we observed coarsening kinetics in $\log(t)$, and we inferred that the dominant growth mechanism of these two species at low ΔT was surface nucleation. Bindeman (2003) drew the same conclusion from the shape of CSDs of quartz phenocrysts in pumices from voluminous ash-flow tuffs. For olivine in a basaltic liquid, the coarsening kinetics in $t^{1/3}$ and the shape of CSDs suggest that olivine grows by a screw dislocation mechanism. These results are in good agreement with theories of crystal growth from the melt (Kirkpatrick 1975, 1981; Dowty 1980), which predict that at very low degrees of undercooling the growth of silicates should be controlled by a layer growth mechanism: surface nucleation or screw dislocation. In a forthcoming paper (Provost et al., in preparation), we combine the experimental results with the analytical and numerical models of Ostwald ripening to estimate the growth rates of olivine, plagioclase, and quartz at $\Delta T \rightarrow 0^{\circ}\text{C}$.

Conclusions

The kinetics of Ostwald ripening in the systems plagioclase-andesite and forsterite-basalt have been determined experimentally. Ostwald ripening of plagioclase is very sluggish and cannot lead to mean grain sizes larger than a few tens of microns, whereas olivine may coarsen to a mean grain size of several hundreds of microns in reasonable durations. In both systems, the kinetics of Ostwald ripening is controlled by the rate of grain growth/dissolution at solid-liquid interfaces, not by diffusion in the liquid. However, the rate-limiting mechanism is different in the two systems: it is surface nucleation in the case of plagioclase, leading to an increase of the mean grain size as $\log(t)$, whereas it is a screw dislocation mechanism in the case of olivine, leading to an increase of the mean grain size as $t^{1/3}$. Ostwald ripening experiments allow to reproduce in the laboratory degrees of undercooling $\Delta T \rightarrow 0^{\circ}\text{C}$. Therefore, this type of experiments may provide a unique opportunity to determine the mechanisms and rates of crystal growth in slowly crystallising magma chambers.

Acknowledgements This manuscript benefited from discussions with Alain Baronnet, Yves Biennu, Albert Jambon, Gilles Quérel, and Daniel Vielzeuf. Michèle Veschambre and Jean-Luc Devidal are thanked for technical assistance with the electron

microprobe, and Pierre Boivin for technical assistance with the 1-atm furnaces. Ilya Bindeman is thanked for its constructive review and Dave Walker for raising the issue of thermal fluctuations in 1-atm furnaces. The authors acknowledge the financial support provided by the Institut National des Sciences de l'Univers (INSU-CNRS). Work supported in part by the European Community's Human Potential Program under contract HPRN-CT-2002-00211 (Research Training Network EUROMELT). Contribution INSU-CNRS 381.

References

- Ardell AJ (1972) The effect of volume fraction on particle coarsening: theoretical considerations. *Acta Metall* 20:61–71
- Baronnet A (1984) Growth kinetics of the silicates. *Fortschr Mineral* 62:187–232
- Bindeman IN (2003) Crystal sizes in evolving silicic magma chambers. *Geology* 31:367–370
- Brailsford AD, Wynblatt P (1979) The dependence of Ostwald ripening kinetics on particle volume fraction. *Acta Metall* 27:489–497
- Brandeis G, Jaupart C, Allègre CJ (1984) Nucleation, crystal growth, and the thermal regime of cooling magmas. *J Geophys Res* 89:10161–10177
- Bulau JR, Waff HS, Tyburczy JA (1979) Mechanical and thermodynamical constraints on fluid distribution in partial melts. *J Geophys Res* 84:6102–6108
- Cabane H (2002) Etude théorique et expérimentale de la cinétique du mûrissement d'Ostwald dans les magmas; implications pour la dynamique des processus magmatiques. PhD Thesis, Université Blaise Pascal
- Cabane H, Laporte D, Provost A (2001) Experimental investigation of the kinetics of Ostwald ripening of quartz in silicic melts. *Contrib Mineral Petrol* 142:361–373
- Chai BHT (1974) Mass transfer of calcite during hydrothermal recrystallization. *Carnegie Inst Washington Pub* 634, Geochemical transport and kinetics, pp 205–218
- Dehoff RT (1984) Generalized microstructural evolution by interface controlled coarsening. *Acta Metall Mater* 32:43–47
- Dehoff RT (1991) A geometrically general theory of diffusion controlled coarsening. *Acta Metall Mater* 39:2349–2360
- Dowty E (1980) Crystal growth and nucleation theory and the numerical simulation of igneous crystallization. In: Hargraves RB (ed) *Physics of magmatic processes*. Princeton University Press, Princeton, pp 419–485
- Gilmer GH (1976) Growth on imperfect crystal faces: I. Monte-Carlo growth rates. *Jour Crystal Growth* 36:15–28
- Green JR, Margerison D (1978) Statistical treatment of experimental data. Elsevier, Amsterdam, p 382
- Higgins MD (1994) Determination of crystal morphology and size from bulk measurements on thin sections: numerical modelling. *Amer Mineral* 79:113–119
- Higgins MD (1998) Origin of anorthosite by textural coarsening: quantitative measurements of a natural sequence of textural development. *J Petrol* 39:1307–1323
- Higgins MD (2000) Measurement of crystal size distributions. *Amer Mineral* 85:1105–1116
- Hort M, Spohn T (1991) Crystallization calculations for a binary melt cooling at constant rates of heat removal: implications for the crystallization of magma bodies. *Earth Planet Sci Lett* 107:463–474
- Jackson K, Uhlmann D, Hunt J (1967) On the nature of crystal growth from the melt. *J Cryst Growth* 1:1–36
- Jambon A, Lussiez P, Clochiatti R, Weisz J, Hernandez J (1992) Olivine growth rates in a tholeiitic basalt: an experimental study of melt inclusions in plagioclase. *Chem Geol* 96:277–287
- Kahlweit M (1975) Ostwald ripening of precipitates. *Adv Colloid Interface Sci* 5:1–35
- Kirkpatrick RJ (1975) Crystal growth from the melt: a review. *Amer Mineral* 60:798–814

- Kirkpatrick RJ (1981) Kinetics of crystallization of igneous rocks. *Mineral Soc Am Rev Mineral* 8:321–398
- Kirkpatrick RJ, Robinson GR, Hayes JF (1976) Kinetics of crystal growth from silicate melts: anorthite and diopside. *J Geophys Res* 81:5715–5720
- Lasaga AC (1998) Reaction kinetics in geosciences. Princeton University Press, Princeton, p 811
- LaTourette T, Wasserburg GJ, Fahey AJ (1996) Self diffusion of Mg, Ca, Ba, Nd, Yb, Ti, Zr, and U in haplobasaltic melt. *Geochim Cosmochim Acta* 60:1329–1340
- Leshner CE, Hervig RL, Tinker D (1996) Self diffusion of network formers (silicon and oxygen) in naturally occurring basaltic liquid. *Geochim Cosmochim Acta* 60:405–413
- Lifshitz IM, Slyozov VV (1961) The kinetics of precipitation from supersaturated solid solutions. *J Phys Chem Solids* 19:35–50
- Marqusee JA, Ross J (1984) Theory of Ostwald ripening: competitive growth and its dependence on volume fraction. *J Chem Phys* 80:536–543
- Marsh BD (1988) Crystal size distribution (CSD) in rocks and the kinetics and dynamics of crystallization: I. Theory. *Contrib Mineral Petrol* 99:277–291
- Marsh BD (1998) On the interpretation of crystal size distributions in magmatic systems. *J Petrol* 39:553–599
- Muncill GE, Lasaga AC (1987) Crystal-growth kinetics of plagioclase in igneous systems: one-atmosphere experiments and application of a simplified growth model. *Amer Mineral* 72:299–311
- Ostwald W (1901) Über die vermeintliche Isomerie des roten und gelben Quecksilberoxyds und die Oberflächen-spannung Fester Körper. *Z Phys Chem* 34:495–512
- Park Y, Hanson B (1999) Experimental investigation of Ostwald-ripening rates of forsterite in the haplobasaltic system. *J Volcanol Geotherm Res* 90:103–113
- Presnall DC, Dixon SA, Dixon JR, O'Donnel TH, Brenner NL, Schrock RL, Dycus DW (1978) Liquidus phase relations on the join diopside-forsterite-anorthite from 1 atm to 20 kbars: their bearing on the generation and crystallization of basaltic magma. *Contrib Mineral Petrol* 66:203–220
- Ratke L, Uffelman D, Bender W, Voorhes PW (1995) Theory of Ostwald ripening due to a second-order reaction. *Scripta Metall Mater* 33:363–367
- Russ JC, Dehoff RT (2000) Practical stereology, 2nd edn. Kluwer/Plenum, Dordrecht, New York, p 381
- Saltykov SA (1967) The determination of the size distribution of particles in an opaque material from the measurement of the size distribution of their sections. In: Helias H (ed) *Stereology*, Springer, Berlin Heidelberg New York, pp 163–173
- Solomatov VS, Stevenson DJ (1993) Kinetics of crystal growth in a terrestrial magma ocean. *J Geophys Res* 98:5407–5418
- Wagner C (1961) Theorie der Alterung von Niederschlägen durch Umlösen. *Z Elektrochem* 65:581–591
- Walker D, Jurewicz SR, Watson EB (1988) Accumulus dunite growth in a laboratory thermal gradient. *Contrib Mineral Petrol* 99:306–319
- Watanabe K, Kitamura M (1992) Growth mechanisms of plagioclase in a basaltic melt. *Mineral J* 16:201–214
- Weill DF, Hon R, Navrotsky A (1980) The igneous system CaMgSi₂O₆-CaAl₂Si₂O₈-NaAlSi₃O₈: variations on a classic theme by Bowen. In: Hargraves RB (ed) *Physics of magmatic processes*. Princeton University Press, Princeton, pp 49–92
- Worster MG, Huppert HE, Sparks RSJ (1990) Convection and crystallization in magma cooled from above. *Earth Planet Sci Lett* 101:78–89
- Zhang Y, Walker D, Leshner CE (1989) Diffusive crystal dissolution. *Contrib Mineral Petrol* 102:492–513